1521-0111/89/4/425–434$25.00
MOLECULAR PHARMACOLOGY

http://dx.doi.org/10.1124/mol.115.102798
Mol Pharmacol 89:425–434, April 2016

Targeting Nonsquamous Nonsmall Cell Lung Cancer via the Proton-Coupled Folate Transporter with 6-Substituted Pyrrolo [2,3-*d*]Pyrimidine Thienoyl Antifolates [S]

Mike R. Wilson, Zhanjun Hou, Si Yang, Lisa Polin, Juiwanna Kushner, Kathryn White, Jenny Huang, Manohar Ratnam, Aleem Gangjee,[1] and Larry H. Matherly[1]

Department of Oncology (M.R.W., Z.H., L.P., J.K., K.W., J.H., M.R., L.H.M.), and Department of Pharmacology (L.H.M.), Wayne State University School of Medicine, Detroit, Michigan; Molecular Therapeutics Program, Barbara Ann Karmanos Cancer Institute, Detroit, Michigan (Z.H., L.P., M.R., L.H.M.); and Division of Medicinal Chemistry, Graduate School of Pharmaceutical Science, Duquesne University, Pittsburgh, Pennsylvania (S.Y., A.G.)

Received December 2, 2015; accepted January 29, 2016

ABSTRACT

Pemetrexed (PMX) is a 5-substituted pyrrolo[2,3-*d*]pyrimidine antifolate used for therapy of nonsquamous nonsmall cell lung cancer (NS-NSCLC). PMX is transported by the reduced folate carrier (RFC) and proton-coupled folate transporter (PCFT). Unlike RFC, PCFT is active at acidic pH levels characterizing the tumor microenvironment. By real-time reverse-transcription polymerase chain reaction (RT-PCR) and immunohistochemistry, PCFT transcripts and proteins were detected in primary NS-NSCLC specimens. In six NS-NSCLC cell lines (A549, H1437, H460, H1299, H1650, and H2030), PCFT transcripts and proteins were detected by real-time RT-PCR and western blots, respectively. 6-Substituted pyrrolo[2,3-*d*]pyrimidine thienoyl antifolates related to PMX [compound 1 (C1) and compound 2 (C2), respectively] are selective substrates for PCFT over RFC. In the NS-NSCLC cell lines, both [^{3}H]PMX and [^{3}H]C2 were transported by PCFT. C1 and C2 inhibited proliferation of the NS-NSCLC cell lines; A549, H460, and H2030 cells were more sensitive to C1 than to PMX. C1 and C2 inhibited glycinamide ribonucleotide formyltransferase in de novo purine nucleotide biosynthesis. When treated at pH 6.8, which favors PCFT uptake, C1 and C2 inhibited clonogenicity of H460 cells greater than PMX; PMX inhibited clonogenicity more than C1 or C2 at pH 7.2, which favors RFC transport over PCFT. Knockdown of PCFT in H460 cells resulted in decreased [^{3}H]PMX and [^{3}H]C2 transport and decreased growth inhibition by C1 and C2, and to a lesser extent by PMX. In vivo efficacy of C1 was seen toward H460 tumor xenografts in severe-combined immunodeficient mice. Our results suggest that 6-substituted pyrrolo[2,3-*d*] pyrimidine thienoyl antifolates offer significant promise for treating NS-NSCLC by selective uptake by PCFT.

Introduction

Nonsmall cell lung cancer (NSCLC) is the leading cause of cancer-related deaths in the United States, accounting for 85% of all diagnosed lung cancers and resulting in over 100,000 deaths per year (American Cancer Society, 2016). Pemetrexed (PMX) is a 5-substituted pyrrolo[2,3-*d*]pyrimidine antifolate (Fig. 1) (Chattopadhyay et al., 2007) and is an important first-line and maintenance therapy in the treatment of nonsquamous (NS)-NSCLC, although patient responses are variable (Esteban et al., 2009; Genova et al., 2013; Gerber and Schiller, 2013; Tomasini et al., 2013). Cellular uptake of folates and classic antifolates is primarily via the facilitative folate transporters, the reduced folate carrier (RFC), and the proton-coupled folate transporter (PCFT) (Matherly et al., 2014). Folate receptor α (FRα) is expressed in some malignancies including NSCLC (Nunez et al., 2012; O'Shannessy et al., 2012; Christoph et al., 2013) and is being exploited for targeted drug delivery (Xia and Low, 2010; Assaraf et al., 2014). However, FRα levels in NS-NSCLC can be variable (Nunez et al., 2012; O'Shannessy et al., 2012; Christoph et al., 2013), at least in part reflecting epidermal growth factor receptor (EGFR) mutation status (Nunez et al., 2012) or stage of disease (O'Shannessy et al., 2012), with the highest levels in a subset of specimens. RFC is a ubiquitously expressed folate/anion antiporter, and is widely considered to be the major tissue transporter of folate cofactors and antifolates such as

This study was supported by grants from the National Institutes of Health National Cancer Institute [Grants R01 CA53535, R01 CA152316, and R01 CA125153]; the Eunice and Milt Ring Endowed Chair for Cancer Research (L.H.M.); and the Duquesne University Adrian Van Kaam Chair in Scholarly Excellence (A.G.). The Barbara Ann Karmanos Cancer Institute provided pilot project funds for the immunohistochemistry studies. M.R.W. was supported by a training grant from the National Institutes of Health [Grant T32 CA009531].
[1]A.G. and L.H.M. contributed equally to this work.
dx.doi.org/10.1124/mol.115.102798.
[S] This article has supplemental material available at molpharm.aspetjournals.org.

ABBREVIATIONS: ALK, anaplastic lymphoma tyrosine kinase; C1, compound 1; C2, compound 2; EGFR, epidermal growth factor receptor; FPGS, folylpolyglutamate synthetase; FRα, folate receptor α; GARFTase, glycinamide ribonucleotide formyltransferase; IHC, immunohistochemistry; KD, knockdown; NS, nonsquamous; NSCLC, nonsmall cell lung cancer; NTC, nontargeted control; PBS, phosphate-buffered saline; PCFT, proton-coupled folate transporter; PCR, polymerase chain reaction; PMX, pemetrexed; RFC, reduced folate carrier; RT, reverse-transcription; SCID, severe-combined immunodeficient; TS, thymidylate synthase.

methotrexate and PMX (Matherly et al., 2007). PCFT was identified in 2006 as a folate/proton symporter with an acidic pH optimum and was localized to the upper gastrointestinal tract where it transports dietary folates across the apical brush border of the small intestine (Qiu et al., 2006). Although other tissues such as liver and kidney also express PCFT (Desmoulin et al., 2012a), in these tissues its biologic role is less certain since the neutral pH microenvironment is not conducive to high levels of PCFT transport (Zhao et al., 2009). PCFT is commonly expressed in human tumor cells including NS-NSCLC cell lines (Kugel Desmoulin et al., 2011), and likely facilitates PMX uptake and contributes to antitumor efficacy with this disease since the acidic microenvironment of tumors greatly favors transport by PCFT over RFC (Zhao and Goldman, 2007; Desmoulin et al., 2012a).

Once internalized, PMX is metabolized to polyglutamates by folylpolyglutamate synthetase (FPGS), resulting in drug forms with enhanced cellular retention over nonpolyglutamyl PMX and increased binding affinities for intracellular enzyme targets (Chattopadhyay et al., 2007). Thymidylate synthase (TS) is the primary intracellular enzyme target for PMX (Chattopadhyay et al., 2007) and TS levels have been implicated in some studies as an important determinant of PMX clinical response, such that tumors with highly elevated TS would be expected to show PMX resistance (Christoph et al., 2013; Liu et al., 2013). At least some of the variable responses to PMX seen clinically may reflect an impact of coadministering dexamethasone with PMX to alleviate possible side effects since dexamethasone attenuates PMX cytotoxicity in NS-NSCLC cells by reversibly blocking cell cycle progression, secondary to the presence of high levels of the glucocorticoid receptor α (Patki et al., 2014). Interestingly, dexamethasone treatment of NS-NSCLC cells in vitro also resulted in reduced expression of RFC and PCFT (Patki et al., 2014). PMX can inhibit folate-dependent enzymes other than TS, including glycinamide ribonucleotide formyltransferase (GARFTase) and 5-aminoimidazole-4-carboxamide ribonucleotide formyltransferase in de novo purine nucleotide biosynthesis (Shih and Thornton, 1999; Racanelli et al., 2009).

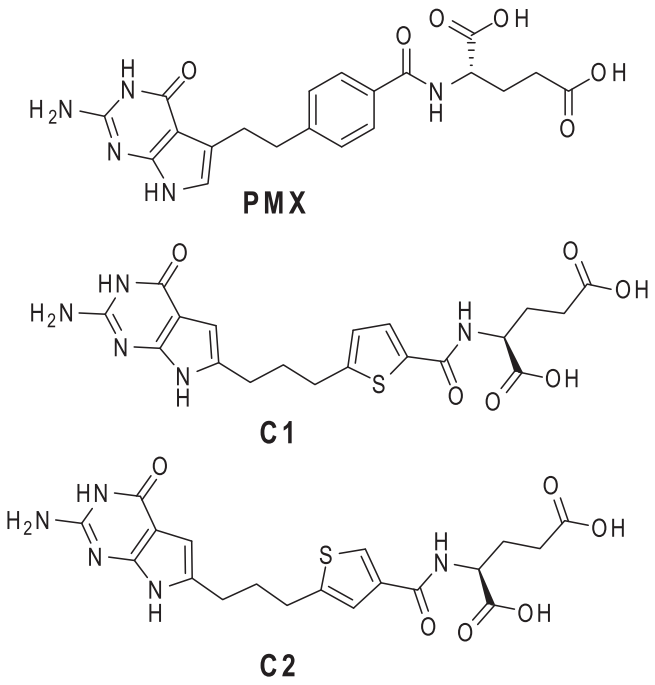

Fig. 1. Structures of PMX, C1, and C2. (A) Structures are shown for PMX and 6-substituted pyrrolo[2,3-*d*]pyrimidine thienoyl antifolate C1 and C2.

Given variable patient responses to PMX, another promising strategy is to develop analogs with increased selectivity for membrane transport by PCFT over RFC, thus increasing specificity toward tumors, while decreasing toxicity toward normal tissues (Desmoulin et al., 2012a). Ideally, these agents would target intracellular enzymes other than TS, thus potentially circumventing PMX resistance due to TS alterations.

The synthesis and biologic activities of a novel series of 2′,4′ and 2′,5′ thienoyl 6-substituted pyrrolo[2,3-*d*]pyrimidine antifolates, typified by compound 1 (C1), AGF94, and compound 2 (C2), AGF154 (Fig. 1), have been previously described (Wang et al., 2011, 2015; Desmoulin et al., 2012b; Cherian et al., 2013). C1 and C2 exhibit transport specificity for PCFT over RFC and deplete purine nucleotides due to inhibition of de novo biosynthesis at GARFTase, the first folate-dependent step. Although GARFTase inhibitors have been previously described (i.e., lometrexol, AG2034) (Boritzki et al., 1996; Mendelsohn et al., 1999) and have shown potent antitumor effects, this was accompanied by unacceptable levels of toxicity in patients (Ray et al., 1993; Budman et al., 2001). This problem may be overcome by combining GARFTase targeting and PCFT transport selectivity, which characterizes antifolates such as C1 and C2. In this study, we explore the therapeutic potential of these novel tumor-targeted 6-substituted pyrrolo [2,3-*d*]pyrimidine antifolates with selective membrane transport by PCFT over RFC in NS-NSCLC.

Materials and Methods

Reagents. The 6-substituted pyrrolo[2,3-*d*]pyrimidine antifolates C1 [(*S*)-2-({5-[3-(2-amino-4-oxo-4,7-dihydro-3H-pyrrolo[2,3-*d*]pyrimidin-6-yl)-propyl]-thiophene-2-carbonyl}-amino)-pentanedioic acid] and C2 [(*S*)-2-({5-[3-(2-amino-4-oxo-4,7-dihydro-3H-pyrrolo[2,3-*d*]-pyrimidin-6-yl)-propyl]-thiophene-3-carbonyl}-amino)-pentanedioic acid] were synthesized as previously described (Wang et al., 2011, 2015). PMX [*N*-(4-[2-(2-amino-3,4-dihydro-4-oxo-7*H*-pyrrolo[2,3-*d*]pyrimidin-5-yl) ethyl]benzoyl)-L-glutamic acid] (Alimta) was obtained from Eli Lilly and Co. (Indianapolis, IN). PT523 [N^{α}-(4-amino-4-deoxypteroyl)-N^{δ}-hemiphthaloyl-L-ornithine) (Rosowsky et al., 1994) was a gift of Dr. A. Rosowsky (Boston, MA). Leucovorin [(6R,*S*) 5-formyl tetrahydrofolate] was obtained from the Drug Development Branch, National Cancer Institute, Bethesda, MD. [^{3}H]PMX (87 Ci/mmol), [^{3}H]C2 (12.3 Ci/mmol), and [^{14}C(U)]glycine (87mCi/mmol) were purchased from Moravek Biochemicals (Brea, CA). Other chemicals were obtained from commercial sources in the highest available purity.

Real-Time Reverse-Transcription Polymerase Chain Reaction (RT-PCR) Analysis of Folate-Related Transcripts. Patient cDNAs were purchased from Origene (Rockville, MD), including 26 NS-NSCLC specimens (8, stage I; 5, stage II; 7, stage III; and 6, stage IV) and eight unmatched normal lung specimens. RNAs were isolated from the NS-NSCLC cell lines using TRIzol reagent (Invitrogen, Carlsbad, CA). cDNAs were synthesized with random hexamers and MuLV reverse transcriptase (including RNase inhibitor) (Applied Biosystems, Waltham, MA) and were purified using a QIAquick PCR Purification Kit (QIAGEN, Valencia, CA). Quantitative real-time RT-PCR was performed using a Roche LightCycler 480 (Roche Diagnostics, Indianapolis, IN) with gene-specific primers and FastStart DNA Master SYBR Green I Reaction Mix (Roche Diagnostics). Primer sequences are available

upon request. Transcript levels were normalized to transcript levels of β-actin.

Immunohistochemistry (IHC). The tissue microarray (BC041115b) and IHC services were purchased from US Biomax, Inc. (Rockville, MD). The array included 61 NS-NSCLC specimens (25, stage I; 19, stage II; 16, stage III; and 1, stage IV) and 10 unmatched normal lung tissues. The tissues were formalin-fixed and paraffin-embedded. The tissue microarrays were deparafinized, rinsed, microwaved, and incubated with polyclonal antibody to human PCFT raised in rabbits (Hou et al., 2012). The serum was purified using a peptide affinity column synthesized from Affi-Gel 10 (BioRad, Richmond, CA). The slides were developed with ImmPRESS anti-Rabbit IgG (peroxidase) (Vector Laboratories, Burlingam, CA) and peroxidase substrate 3,3′-diaminobenzidine tetrahydrochloride, and then rinsed, counterstained with Hematoxylin QS (Vector Laboratories), cleared, and mounted with permanent mounting medium (C0487; Sigma-Aldrich, St. Louis, MO). The slides were manually scored by two independent pathologists with the intensities scored as negative (0), weak (1+), moderate (2+), or strong (3+), and then scanned by an Aperio Image Scanner (Aperio Technologies, Inc., Vista, CA) for microarray image scanning. The total positive cell numbers and intensity of antibody staining of each tissue core were computed.

Cell Culture Conditions. NS-NSCLC cell lines, including A549, H1437, H460, H1299, H1650, and H2030, were obtained from the American Type Culture Collection (Manassas, VA). The identities of the NS-NSCLC cell lines were verified by Genetica DNA Laboratories (Burlington, NC). HeLa cells were gifts from Dr. I. David Goldman (Bronx, NY). Prior to experiments, all cell lines were grown in folate-free RPMI 1640 supplemented with 10% dialyzed fetal bovine serum (Sigma-Aldrich), 1% penicillin/streptomycin, 2 mM L-glutamine, and 25 nM leucovorin for at least 2 weeks.

For growth inhibition assays, the NS-NSCLC cell lines were plated in 96-well culture dishes (1500–4000 cells/well; 200 μl/well) in the aforementioned medium with drug concentrations from 1 to 1000 nM PMX, C1, or C2. Cells were incubated from 96 to 120 hours (depending on the cell line) at 37°C in a CO_2 incubator. Cell viabilities were measured with a fluorescence-based viability assay (CellTiter Blue; Promega, Madison, WI) and a fluorescence plate reader (emission at 590 nm; excitation at 560 nm) to determine drug concentrations that inhibit growth by 50% (IC_{50}). To confirm the targeted pathways and enzymes, proliferation assays were performed with H460 cells treated with PMX, C1, or C2 in the presence of adenosine (60 μM), thymidine (10 μM), or 5-aminoimidazole-4-carboxamide (320 μM) (Wang et al., 2011, 2015).

For colony-forming assays, H460 cells (100–150 cells) in log phase were plated into 60-mm dishes in folate-free RPMI 1640 medium (pH 7.2), supplemented with 25 nM leucovorin, 10% dialyzed fetal bovine serum, 1% penicillin/streptomycin, and 2 mM L-glutamine, and then allowed to adhere for 24 hours. Cells were then treated with drugs in the aforementioned media at pH 6.8 or 7.2. For treatments at pH 6.8, 25 mM 1,4-piperazinediethanesulfonic acid/25 mM HEPES was added (Kugel Desmoulin et al., 2011). After 24 hours, cells were rinsed with Dulbecco's phosphate-buffered saline (PBS), and then incubated in drug-free, folate-free RPMI 1640 medium (pH 7.2) plus dialyzed fetal bovine serum and antibiotics, supplemented with 25 nM leucovorin. After 9 days, the dishes were washed with PBS, 5% trichloroacetic acid, and then with borate buffer (10 mM, pH 8.8), followed by 1% methylene blue (in borate buffer). Dishes were again rinsed with borate buffer, and colonies were counted in order to calculate the percent colony formation relative to the vehicle (e.g., dimethylsulfoxide) control.

Development of H460 PCFT Knockdown (KD) Cell Line. H460 cells were seeded at 2×10^5 cells per well in 24-well plates containing RPMI 1640 (pH 7.2), supplemented with 10% fetal bovine serum, 1% penicillin/streptomycin, and 2 mM L-glutamine, with the addition of 4 μg/ml polybrene and 10^5 transducing units of MISSION Lentiviral particles (Sigma-Aldrich) containing shRNA targeting PCFT or a nontargeted control (NTC) shRNA sequence. After 24 hours, fresh medium including 2 μg/ml puromycin as a selection marker was added. Confluent cultures were trypsinized and passaged 3 to 4 times in the presence of 2 μg/ml puromycin, and then plated in 60-mm dishes in complete medium with 2 μg/ml puromycin at a density of 100 cells/dish to isolate single clones. Clones were picked and expanded and RNAs were isolated to determine the extent of PCFT knockdown by real-time RT-PCR (described previously). Two PCFT KD clones were isolated, designated as KD-3 and KD-4. Altogether, five shRNAs were tested, of which only one (TRCN0000437092) gave >50% knockdown for PCFT.

Gel Electrophoresis and Western Blotting. The NS-NSCLC cell lines were cultured, as described previously. The cells were disrupted by sonication, cell debris was removed by centrifugation (1800 rpm, 5 minutes), and a particulate membrane fraction was prepared by centrifugation at 37,000*g*. The membrane pellet was solubilized with 1% SDS in 10 mM Tris-HCl (pH 7), containing protease inhibitors (Roche Diagnostics). Membrane proteins (30 μg) were electrophoresed on 7.5% polyacrylamide gels with SDS (Laemmli, 1970) and transferred to polyvinylidene difluoride membranes (Thermo Fisher Scientific, Waltham, MA) (Matsudaira, 1987). To detect PCFT, human PCFT-specific polyclonal antibody raised in rabbits to a carboxyl termini peptide (Hou et al., 2012) was used, with IRDye800CW-conjugated goat anti-rabbit IgG secondary antibody (LICOR Biosciences, Omaha, NE). Membranes were scanned and densitometry was performed with an Odyssey infrared imaging system (LICOR Biosciences). Protein loading was normalized to levels of β-actin using anti-β-actin mouse antibody (Sigma-Aldrich).

Antifolate Transport Assays. Transport assays were performed essentially as described previously (Desmoulin et al., 2010, 2012b; Kugel Desmoulin et al., 2011). For transport assays, the NS-NSCLC cell lines were plated at 30%–40% confluence into 60-mm dishes containing complete folate-free RPMI 1640 supplemented with 25 nM leucovorin. After 48 hours, cellular uptakes of [^{3}H]PMX and [^{3}H]C2 (both at 0.5 μM) were measured over 5 minutes (NS-NSCLC cell lines) or 2 minutes (PCFT KD cell lines) at 37°C in 60-mm dishes in 4-morpholineethanesulfonic acid-buffered saline (20 mM 4-morpholineethanesulfonic acid, 140 mM NaCl, 5 mM KCl, 2 mM $MgCl_2$, and 5 mM glucose; pH 5.5). The dishes were washed three times with PBS and cells were solubilized in 0.5 N NaOH. Intracellular radioactivity was calculated as pmol/mg of protein, based on measurements of radioactivity and protein concentrations of the alkaline cell homogenates. To confirm PCFT-mediated transport activity, 10 μM nonradioactive C1 was added to the transport incubations to block uptake.

In Situ GARFTase Enzyme Inhibition Assay. Incorporation of [^{14}C(U)]glycine into [^{14}C]formyl glycinamide ribonucleotide, as an in situ measure of intracellular GARFTase activity in folate-depleted H460 cells at pH 6.8, was performed exactly as previously described (Desmoulin et al., 2010; Wang et al., 2011). Results were expressed as pmol/mg protein. Drug-treated samples were normalized to untreated controls to calculate the IC_{50} values.

In Vivo Antitumor Efficacy of C1 toward H460 Xenografts in Severe-Combined Immunodeficient (SCID) Mice. Cultured H460 cells were implanted subcutaneously (10^7 cells/flank) into female ICR SCID mice (National Institutes of Health DCT/DTP Animal Production Program, Frederick, MD) to develop a solid tumor xenograft model (passage 0). Mice were supplied water and food ad libitum. Study mice were maintained on a folate-deficient diet (TD.00434; Harlan Teklad, Madison, WI) starting 14 days prior to tumor implant to ensure that serum folate levels approximated those of humans before the start of therapy (Wang et al., 2010, 2011; Cherian et al., 2013). Serum folate assays (Varela-Moreiras and Selhub, 1992) were performed just prior to tumor engraftment and were repeated at the conclusion of the drug treatments. This design is analogous to those previously published (Alati et al., 1996; Gibbs et al., 2005).

To test drug efficacy, experimental mice were pooled, divided into groups (five mice/group), and bilaterally implanted subcutaneously with 30–60 mg H460 tumor fragments, using a 12-gauge trocar (day 0).

Chemotherapy began on day 1 after tumor implantation, when the number of cells was between 10^7 and 10^8 cells (below the limit of palpation). Organic solvent (ethanol, 5% v/v), carrier (Tween 80, 1% v/v), and sodium bicarbonate (0.5% v/v) were used to effect solubilization of C1, while cisplatin and gemcitabine were dissolved in sterile saline. All drugs were administered intravenously using an injection volume of 0.2 ml. Mice were weighed daily and tumor measurements were determined using a caliper two-to-three times weekly. Mice were sacrificed when their individual tumor burdens reached 1500 mg (asymptomatic). Mice were necropsied and tissue was harvested to evaluate potential organ-related toxicities (by H&E staining).

Methods for protocol design, drug treatments, toxicity evaluation, and data analysis were previously described (Corbett et al., 1997, 1998; Polin et al., 1997, 2011). Experimental parameters as qualitative and quantitative end points to assess antitumor activities include: T/C (as a percentage) and T–C (tumor growth delay) [where T is the median time (days) required for the treatment group tumors to reach a predetermined size (e.g., 1000 mg) and C is the median time (days) for the control tumors to reach the same size; tumor-free survivors are excluded from these calculations]; and tumor cell kill [$\log_{10}$ cell kill total (gross) = (T–C)/(3.32)(T_d), where (T–C) is the tumor growth delay, as described previously, and T_d is the tumor volume doubling time (days), estimated from the best-fit straight line from a log-linear growth plot of control group tumors in exponential growth (100–800 mg)]. For comparisons of antitumor activities with standard agents or between tumors, $\log_{10}$ kill values were converted to an arbitrary activity rating (Corbett et al., 1997). With the exception of the H460 xenograft cell line and the drugs used in treatment, these methods are identical to those described previously (Wang et al., 2010, 2011, 2015; Cherian et al., 2013).

Statistical Analysis. Descriptive statistical tests (e.g., *t* tests) were conducted using GraphPad 6.0 software (La Jolla, CA).

Results

Expression Profiles for Folate Transport and Metabolism Genes in NS-NSCLC Patient Specimens. To begin to identify key determinants of antitumor efficacy of the 2′,4′, and 2′,5′ thienoyl pyrrolo[2,3-*d*]pyrimidine antifolates C1 and C2 (Fig. 1) toward NS-NSCLC, we measured PCFT transcripts (by real-time RT-PCR) and proteins (by IHC) in NS-NSCLC and unmatched (i.e., from different patients) normal lung specimens (Fig. 2). Clinical specimens were obtained from different commercial sources such that PCFT gene expression and protein levels could not be directly compared for individual samples.

PCFT transcripts were similarly expressed (based on median values) in 26 NS-NSCLC and 8 normal lung specimens, although the range was much broader in the former (16- versus 3-fold, respectively) (Fig. 2A). By IHC, PCFT proteins were substantially increased (3.8-fold) in NS-NSCLC specimens ($n = 61$) over normal lung ($n = 10$) ($P < 0.001$) and again showed a broad expression pattern (~150-fold for NS-NSCLC and ~4-fold for normal lung, respectively) (Fig. 2B). Representative IHC sections for NS-NSCLC specimens expressing low, intermediate, and high PCFT levels are shown in Fig. 2C. Histopathological and clinical information for tissue microarray specimens along with PCFT quantitation are summarized in Supplemental Material (Table S1). For both RT-PCR and IHC analyses, there were no significant changes in PCFT levels with tumor stage.

Transcript levels for other genes relevant to antitumor efficacy of this series of compounds were also measured in the clinical specimens, including folate transporters (RFC, FRα) and metabolism enzymes (TS, GARFTase, and FPGS) (Supplemental Material; Figure S1). Transcripts for all these genes were detected. Transcript levels were increased in NS-NSCLC ($n = 26$) compared with normal lung ($n = 8$) for TS (median 2.25-fold increased; $P = 0.015$) and GARFTase (median ~2-fold increased; $P < 0.0001$). Slightly decreased median RFC transcript levels (2.64-fold; $P = 0.016$) were measured in the NS-NSCLC specimens. Although median FRα and FPGS levels were unchanged between NS-NSCLC and normal lung specimens, the range was much broader for the tumors (from 13-fold for FPGS and ~2000-fold for FRα, compared with 2- to 3-fold for normal lung for both FPGS and FRα). Collectively, these results establish high-level expression of PCFT in NS-NSCLC, along with appreciable expression of other folate-related genes. Although FRα is expressed in NS-NSCLC, its levels were highly variable.

Expression Profiles for Folate Transport and Metabolism Genes in NS-NSCLC Cell Lines. We extended our gene expression analysis to NS-NSCLC cell lines, including A549, H1437, H460, H1299, H1650, and H2030. For these experiments, HeLa cells were used as a positive control since HeLa cells express abundant RFC and PCFT accompanying

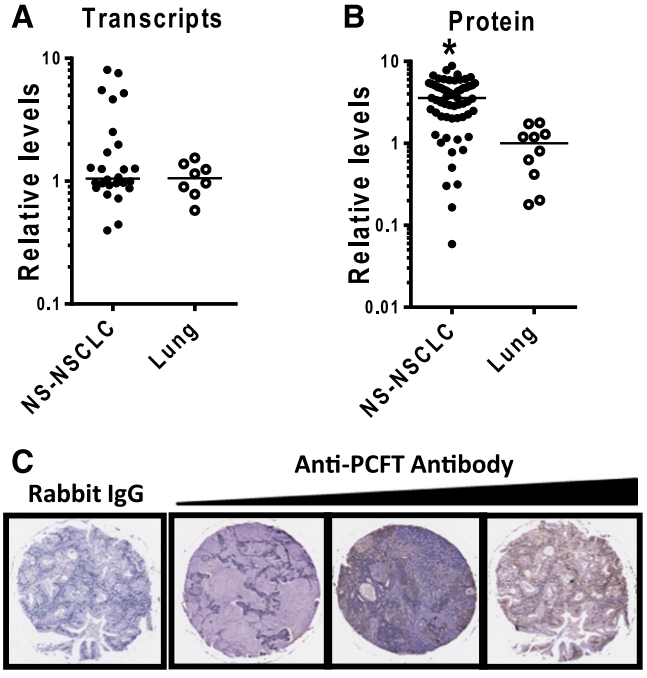

Fig. 2. PCFT expression in primary NS-NSCLC and normal lung specimens. (A) Results for quantitative real-time RT-PCR are shown for 26 NS-NSCLC and 8 normal lung specimens (Origene). PCFT transcript levels were normalized to transcript levels for β-actin. The median value for the normal lung specimens was assigned a value of 1. (B and C) IHC results are shown for 61 NS-NSCLC and 10 normal lung tissues from a tissue microarray (TMA) (US Biomax, Inc.). The TMA was incubated with affinity-purified PCFT-specific antibody or rabbit IgG, and the slides were developed, counterstained, and mounted, as described in *Materials and Methods*. Representative images are shown in (C) for IgG and for three NS-NSCLC specimens with low-, intermediate-, and high-level staining (left to right). The slides were scanned by an Aperio Image Scanner (Aperio Technologies, Inc.) for microarray image scanning. The total positive cell numbers and intensity of antibody staining of each tissue core were computed and are shown in (B). The median value for the normal lung specimens was assigned a value of 1. Statistical significance between the groups was analyzed by the student's *t* test. An asterisk indicates a statistically significant difference between the median NS-NSCLC value and the median value for the normal lung specimens ($P < 0.001$).

low levels of FRα (Kugel Desmoulin et al., 2011). PCFT was expressed in the six NS-NSCLC cell lines over a ~13-fold range, with the highest transcript levels in A549 cells and a very low level in H1299 cells (Fig. 3A). Correlations between levels of PCFT transcripts by real-time RT-PCR and PCFT proteins on western blots probed with PCFT antibody (Fig. 3B) were inexact. For H1299 cells, PCFT protein was undetectable. FRα was undetectable in five out of six of the NS-NSCLC cell lines, the only exception being the H1437 cell line (expresses ~9% of the FRα levels in HeLa cells) (Supplemental Material; Figure S2). RFC, TS, GARFTase and FPGS transcripts were expressed at similar levels among the various NS-NSCLC cell lines (Supplemental Material; Figure S2).

PMX and C2 Transport by PCFT in NS-NSCLC Cell Lines. The 5-substituted pyrrolo[2,3-*d*]pyrimidine antifolate PMX is a transport substrate for both RFC and PCFT (Matherly et al., 2014). Unlike PMX, the 6-pyrrolo[2,3-*d*] pyrimidine thienoyl analogs C1 and C2 are highly selective transport substrates for PCFT over RFC, although both are also FRα substrates (Wang et al., 2011, 2015; Desmoulin et al., 2012b; Cherian et al., 2013). To demonstrate that the PCFT proteins detected on western blots in A549, H1437, H460, H1650, and H2030 NS-NSCLC cell lines could transport [^{3}H]PMX and [^{3}H]C2, we measured cellular uptake of these compounds (both at 0.5 μM; 5 minutes; 37°C) at pH 5.5, the PCFT pH optimum. An excess (10 μM) of unlabeled C1 was added as a competitive inhibitor of PCFT to confirm the PCFT-specific uptake component.

The NS-NSCLC cell lines accumulated [^{3}H]PMX and [^{3}H]C2 over 5 minutes to generally similar extents (Fig. 3, C and D), but only partially reflected levels of PCFT proteins (Fig. 3B). For instance, PCFT proteins were generally proportional to transport of both [^{3}H]PMX and [^{3}H]C2 for the H1437, H460, H1299, H1650, and H2030 cell lines; however, transport was disproportionately low for A549 cells. For both [^{3}H]PMX and [^{3}H]C2, uptake was blocked (~80%–95%) by nonradioactive C1. For PCFT-selective [^{3}H]C2, uptake for five of the NS-NSCLC cell lines far exceeded the low residual level measured in the H1299 cells ($P < 0.05$).

Antiproliferative and Cytotoxic Activities of 6-Substituted Pyrrolo[2,3-*d*]Pyrimidine Thienoyl Antifolates C1 and C2 toward NS-NSCLC Sublines Reflect Inhibition of GARFTase in De Novo Purine Nucleotide Biosynthesis. To evaluate the antiproliferative potencies of the 6-substituted pyrrolo[2,3-*d*]pyrimidine thienoyl antifolates C1 and C2 compared with PMX toward the NS-NSCLC cell lines, we performed cell outgrowth assays. Cells were treated in the presence of the drugs for 4 to 5 days and cell proliferation was assayed with a fluorescence-based assay (i.e., CellTiter Blue) to calculate the IC_{50} values corresponding to drug concentrations that inhibit growth by 50%. Under these conditions, the pH of the culture medium decreased to ~pH 6.7–6.8 (Desmoulin et al., 2010). The NS-NSCLC cell lines were sensitive to C1 and C2 (Fig. 4A), with C1 IC_{50} values ranging from 45 nM (H1437) to 230 nM (H1299), and C2 IC_{50}s ranging from 79 nM (H1437) to 288 nM (H1299). The PMX IC_{50} values ranged from 43 nM (H1437) to 163 nM (H2030). Interestingly, the A549, H460, and H2030 cell lines were all more sensitive to C1 than to PMX ($P < 0.05$). Resistance of the H1299 cell line to C1 and C2 likely reflects the lack of

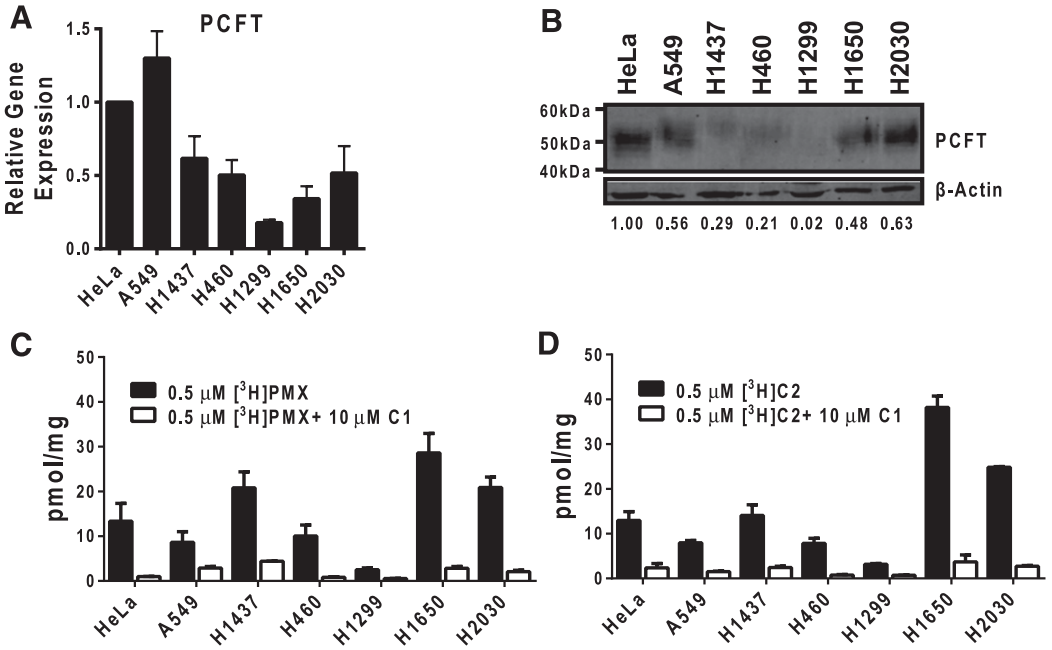

Fig. 3. PCFT expression and function in NS-NSCLC cell lines. (A) Results are shown for PCFT transcript levels measured by real-time RT-PCR in NS-NSCLC cell lines (A549, H1437, H460, H1299, H1650, and H2030). PCFT transcript levels were normalized to transcript levels for β-actin. The PCFT transcript level for the HeLa cell line was assigned a value of 1. Results are shown as mean ± S.E. values from triplicate experiments. (B) Particulate membrane fractions were prepared as described in *Materials and Methods*. Membrane proteins (30 μg) from human tumor cell lines were electrophoresed on a 7.5% polyacrylamide gel and immunoblotted with human PCFT polyclonal antibody. β-Actin levels were used as loading controls. Densitometry was performed using Odyssey software, and PCFT protein expression was normalized to β-actin. Normalized densitometry results (as an average from three experiments) are shown. (C and D) NS-NSCLC cells (in 60-mm dishes) were treated with 0.5 μM [^{3}H]PMX or [^{3}H]C2 at pH 5.5 and 37°C for 5 minutes (black bars). Nonradioactive C1 (10 μM) was added to competitively block PCFT-mediated uptake as a negative control for PCFT transport (white bars). Internalized pmol values of [^{3}H]PMX or [^{3}H]C2 were normalized to total cell proteins and expressed as pmol/mg. Histograms show mean ± S.E. values from triplicate experiments.

detectable PCFT protein (Fig. 3B) and limited PCFT transport (Fig. 3D). Although [^{3}H]PMX uptake by PCFT was also low in H1299 cells (Fig. 3C), this was not manifested as PMX resistance (Fig. 4A), likely reflecting RFC transport of PMX (Matherly et al., 2014).

For additional experiments, we used H460 NS-NSCLC cells, reflecting their moderate and proportional level of PCFT protein and transport (Fig. 3, B–D). In H460 cells, C1 and C2 inhibited de novo purine nucleotide biosynthesis at the step catalyzed by GARFTase, as reflected in protection from growth inhibition by adenosine (60 μM) and 5-aminoimidazole-4-carboxamide (320 μM), but not by thymidine (10 μM) (Supplemental Material; Figure S3). GARFTase inhibition in H460 cells was confirmed with a cell-based in situ assay that measures [^{14}C(U)]glycine incorporation into the GARFTase product, [^{14}C]formyl glycinamide ribonucleotide (Supplemental Material; Figure S3) (Desmoulin et al., 2010; Wang et al., 2011, 2015). IC_{50} values for in situ GARFTase inhibition of 78.9 and 27.1 nM were measured for C1 and C2, respectively. C1 and C2 have been previously described as GARFTase inhibitors in other tumor models (Wang et al., 2011, 2015). By in vitro assays with isolated GARFTase, K_i values of 68 nM for C1 and 11 nM for C2 have been previously reported (Wang et al., 2015), paralleling IC_{50} values from the in situ GARFTase assays in H460 cells.

We assessed cytotoxicity resulting from exposure of H460 cells to C1, C2, or PMX, following treatment with drugs (0.1–10 μM) for 24 hours at pH 6.8 or 7.2 (approximating the microenvironment pH of many solid tumors and normal tissues, respectively) (Gillies et al., 2002; Gallagher et al., 2008; Webb et al., 2011). Cells were then washed with PBS and incubated in drug-free medium for 9 days (at neutral pH), at which time colonies were stained with methylene blue and counted. Both C1 and C2 showed a steep concentration-dependent decrease in colony formation following drug treatments at pH 6.8, with a complete loss of clonogenicity at 10 μM (Fig. 4B). Conversely, while PMX was more active than C1 or C2 at 0.1 μM, the dose-response relationship for PMX at pH 6.8 was shallow and incomplete (~10%), even at 10 μM drug. However, following treatment at pH 7.2, PMX showed a dramatically enhanced dose-responsive decrease in colony formation, whereas C1 and C2 showed progressively impaired responses (Fig. 4C). These results demonstrate selective antitumor efficacy of the novel 6-substituted pyrrolo [2,3-*d*]pyrimidine antifolates C1 and C2 compared with PMX at a pH characterizing the tumor microenvironment versus neutral pH typical of most normal tissues. Collectively, these studies establish that C1 and C2 are cytotoxic toward H460 NS-NSCLC cells associated with inhibition of GARFTase and de novo purine nucleotide biosynthesis.

Impact of Knockdown of PCFT on PMX and C2 Transport and Antitumor Drug Efficacy. The results shown in Fig. 3C and D demonstrate that both [^{3}H]PMX and [^{3}H]C2 are transported by PCFT into the NS-NSCLC cell lines. However, PMX (unlike C2) is also transported by RFC (Matherly et al., 2014). To directly examine the impact of this apparent transport redundancy by PCFT and RFC on PMX cellular uptake and antitumor efficacy compared with C1 and C2, we tested five lentiviral shRNAs for knockdown of PCFT in H460 NS-NSCLC cells. For the shRNA construct with the greatest knockdown, two clonal PCFT KD cell lines, KD-3 and KD-4, were developed, both of which showed significant loss of PCFT gene expression (~2.7- and ~3.3-fold decreases, respectively), compared with NTC cells or wild-type (i.e., nontransduced) H460 cells (Fig. 5A). PCFT protein levels were also reduced in KD-3 and KD-4 sublines (29% and 19% of the NTC level by densitometry) (Fig. 5B). There were no significant differences in transcript levels for RFC, TS, GARFTase, and FPGS between KD and NTC cells (data not shown), suggesting

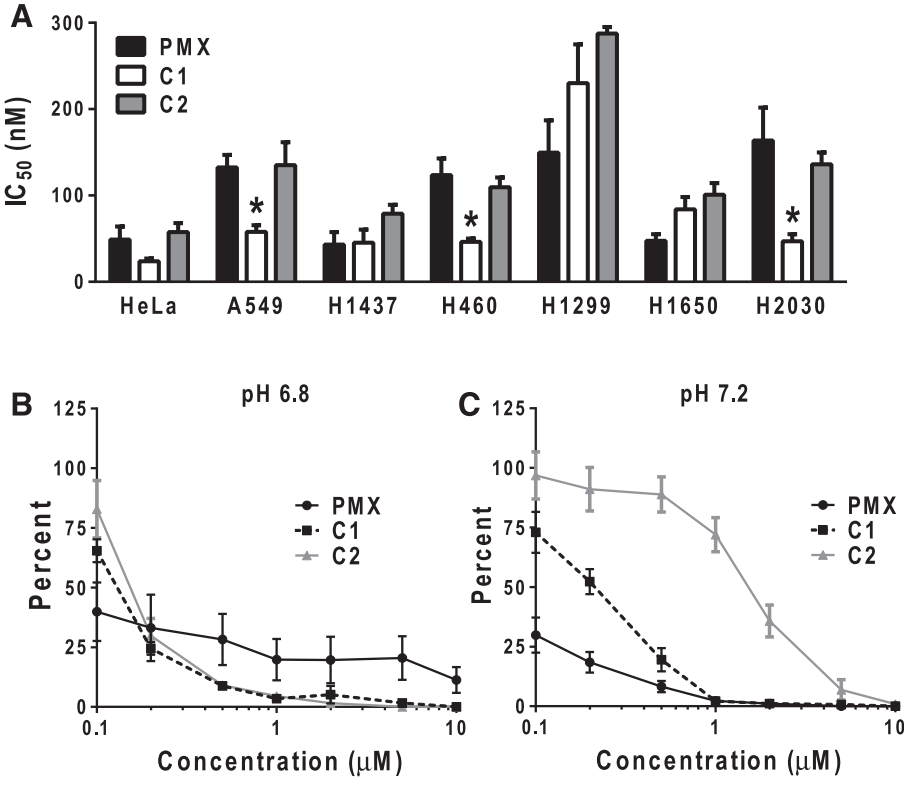

Fig. 4. In vitro drug efficacy of PMX, C1, and C2 of NS-NSCLC cell lines. (A) NS-NSCLC cells were seeded in 96-well plates at 1500–4000 cells/well in complete folate-free RPMI 1640 (pH ~7.2), 10% dialyzed fetal bovine serum, and 25 nM leucovorin. Cells were incubated with varying concentrations of PMX, C1, or C2 from 1 to 1000 nM for 4 to 5 days, depending on the cell line. Cell viabilities were determined with a fluorescence-based assay (Cell Titer Blue). Mean IC_{50} ± S.E. values from triplicate experiments were determined graphically for each drug. Asterisks designate statistically greater sensitivity for C1 compared with PMX ($P < 0.01$). (B and C) H460 cells (100–150 cells) were plated in 60-mm dishes in complete folate-free RPMI 1640 (pH 7.2), 10% dialyzed fetal bovine serum, and 25 nM leucovorin. After 24 hours, cells were then treated with PMX, C1, or C2 at varying concentrations in complete folate-free RPMI 1640 (at pH 7.2 or 6.8) supplemented with 25 nM leucovorin. After an additional 24 hours, cells were rinsed with PBS, and then incubated in complete folate-free RPMI 1640 supplemented with 25 nM leucovorin (pH 7.2) for 9 days. Colonies were stained with methylene blue and counted, and colony numbers were normalized to the controls. Plots show mean ± S.E. values, representative of triplicate experiments.

no significant off-target effects. Furthermore, there were no significant differences in rates of cell proliferation between KD and NTC cells (data not shown).

We also measured PCFT-specific transport activity for KD-3 and KD-4 cells with [^{3}H]PMX and [^{3}H]C2 (both at 0.5 μM) over 2 minutes at 37°C and pH 5.5 in the presence and absence of 10 μM nonradioactive C1 (Fig. 5C and D, respectively). PCFT-selective uptake for both substrates decreased in KD-3 and KD-4 cells compared with the NTC (~70% and ~80% for [^{3}H]C2 and [^{3}H]PMX, respectively, calculated from the difference

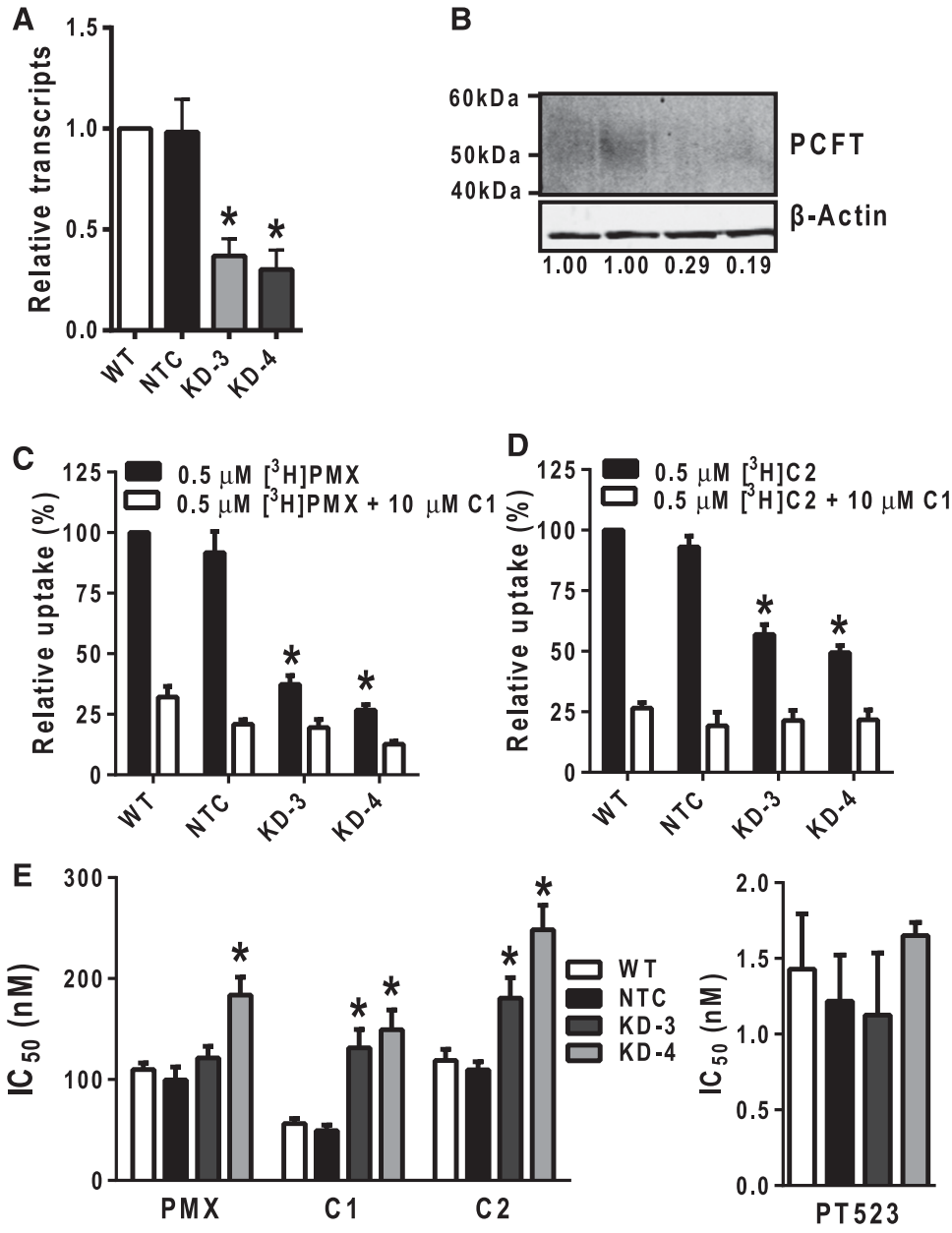

Fig. 5. Characterization of H460 PCFT KD cells. (A) Real-time RT-PCR was used to measure transcript levels for PCFT in H460 wild-type (WT), NTC, KD-3, and KD4 cells. Transcript levels were normalized to β-actin and results are presented relative to those for WT H460 cells (assigned a value of 1). Results are expressed as mean ± S.E. values and represent triplicate experiments. The asterisks indicate a statistically significant difference between the PCFT KD gene expression and that for the NTC cells ($P < 0.05$). (B) H460 particulate membrane fractions were isolated as described in *Materials and Methods*. Membrane proteins (30 μg) from WT, NTC, KD-3, and KD4 H460 cell lines were electrophoresed on a 7.5% polyacrylamide gel and immunoblotted with PCFT antibody. β-Actin protein levels were used as loading controls. Densitometry was measured using Odyssey software, and PCFT protein expression was normalized to β-actin. Normalized densitometry results (average from four experiments) are noted below each lane. (C and D) WT, NTC, KD-3, and KD-4 H460 cells (in 60-mm dishes) were incubated with 0.5 μM [^{3}H]PMX and [^{3}H]C2 at pH 5.5 and 37°C, with or without 10 μM nonradioactive C1 for 2 minutes. Internalized [^{3}H]PMX or [^{3}H]C2 was normalized to total cell protein and results calculated as pmol/mg. Uptake results are presented as relative uptake with WT H460 cells assigned a value of 100%. Results are expressed as mean ± S.E. values, representative of triplicate experiments. The asterisks indicate a statistically significant difference between the PCFT transport activity in the KD (KD-3 and KD-4) cells and that of the NTC cells ($P < 0.05$). (E) The H460 sublines including WT, NTC, KD-3, and KD-4 H460 cells were cultured in complete folate-free RPMI 1640 with 25 nM leucovorin in 96-well plates at 1500 cells/well with varying concentrations of PMX, C1, C2 (left panel), or PT523 (right panel) for 4 days. Viable cells were measured by a fluorescence-based assay (Cell Titer Blue) and IC_{50} values were determined graphically. Results are expressed as mean IC_{50} ± S.E. values from triplicate experiments (the asterisk indicates where IC_{50} values for PCFT KD cells are significantly greater than for NTC; $P < 0.05$).

with and without C1 competitor), paralleling changes in PCFT transcripts and proteins.

To extend these studies to analyses of drug sensitivities, we assessed in vitro antitumor efficacies of PMX, C1, and C2 toward KD-3 and KD-4, compared with NTC and wild-type H460 cells. Results were compared with those for PT523, a RFC-selective antifolate with no PCFT transport activity (Rosowsky et al., 1994; Wang et al., 2010). Both KD and NTC cells were highly sensitive to the growth inhibitory effects of PT523 (Fig. 5E, right panel). In contrast, the IC_{50} values in the KD cells were significantly increased for both C1 (2.7- and 3.0-fold increases for KD-3 and KC-4, respectively) and C2 (1.7- and 2.3-fold increases for KD-3 and KC-4, respectively) (Fig. 5E, left panel). This further establishes the reliance on PCFT membrane transport for C1 and C2 drug efficacy. For PMX, a similar, albeit lesser, impact on drug sensitivity was observed for KD-3 and KD-4 cells (1.2- and 1.8-fold decreases, respectively) (Fig. 5E, left panel), suggesting a reduced dependence on PCFT transport for PMX antitumor efficacy, likely reflecting its RFC substrate activity.

Effects of C1 on NS-NSCLC Tumor Growth In Vivo. To assess antitumor effects of C1 in the context of NS-NSCLC in vivo, we performed antitumor efficacy studies with 8-week-old female ICR SCID mice implanted subcutaneously with H460 tumor fragments. Mice were maintained ad libitum on a folate-deficient diet in order to decrease serum folates to levels approximating those seen in humans (Alati et al., 1996; Wang et al., 2010, 2011, 2015). Control and drug treatment groups were nonselectively randomized (five mice/group), and C1 (32 mg/kg), gemcitabine (125 mg/kg), or cisplatin (2.4 mg/kg) was administered intravenously on days 1, 5, 9, and 13 after tumor implantation. Treatment regimens were based on the efficacious dose range for each of the drugs (i.e., the highest nontoxic total dose range), as tolerated by SCID mice on an every fourth day for four times schedule [the in-house highest nontoxic total dose ranges were as follows: C1 (96–160 mg/kg); gemcitabine (450–750 mg/kg), and cisplatin (8–12 mg/kg)]. Mice were observed and weighed daily; tumors were measured two-to-three times per week.

C1 showed greater efficacy toward H460 xenografts (T/C = 11%; T–C = 9 days; 1.9 gross $\log_{10}$ kill) than either cisplatin (T/C = 28%; T–C = 8 days; 1.7 gross $\log_{10}$ kill) or gemcitabine (T/C = 26%; T–C = 7 days; 1.5 gross $\log_{10}$ kill) (Fig. 6). The drugs appeared to be well tolerated and there was no drug-related lethality. Minimal adverse toxicities occurred and there was no evidence of organ-related toxicities. The only dose-limiting symptom was weight loss. For cisplatin and gemcitabine, mice sustained weight losses of 19.8% with a nadir on days 20–22, and 5.9% with a nadir on day 15, respectively. Full recovery did not occur prior to sacrifice due to the mice reaching the tumor burden limit [94% weight recovery for cisplatin within 4 days postnadir (day 26) and 99% weight recovery for gemcitabine 9 days postnadir (day 24)]. For C1, 14% maximal weight loss was measured on day 7 post-treatment, with full weight recovery by day 16. These results demonstrate potent in vivo efficacy of C1 toward H460 lung cancer xenografts.

Discussion

The potential utility of the 2′,4′, and 2′,5′ thienoyl pyrrolo [2,3-*d*]pyrimidine antifolates, C1 and C2, for selective targeting of ovarian cancer and malignant mesothelioma via FRα and/or PCFT over RFC, has been previously reported (Wang et al., 2011, 2015; Cherian et al., 2013). In the present study, we extended this work to NS-NSCLC, a disease for which PMX is heavily used in both first-line and maintenance therapies (Genova et al., 2013; Gerber and Schiller, 2013; Tomasini et al., 2013). However, only about one-third of patients with NS-NSCLC respond to PMX, such that the median progression-free survival is only ~6 months in the front-line setting, when combined with platinum, and ~4 months as a single agent in patients with recurrent NS-NSCLC (Esteban et al., 2009).

Our investigation of NS-NSCLC clinical specimens and cell lines established that PCFT transcripts and proteins

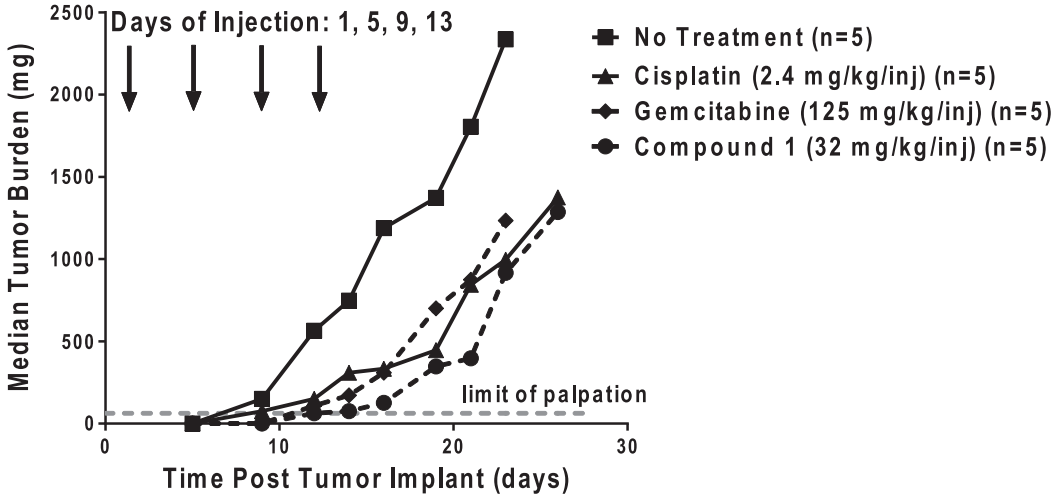

Fig. 6. Analysis of in vivo efficacy of C1. An in vivo efficacy trial of C1 in H460 xenografts was performed. Female ICR SCID mice were maintained on a folate-deficient diet ad libitum. Human H460 tumors were implanted bilaterally and subcutaneously, and mice were nonselectively randomized into five mice per group. C1 [32 mg/kg injection, dissolved in 5% ethanol (v/v), 1% Tween 80 (v/v), and 0.5% $NaHCO_3$], gemcitabine (125 mg/kg injection, dissolved in 0.9% saline), and cisplatin (2.4 mg/kg injection, dissolved in 0.9% saline) were administered on a schedule of every 4 days for four intravenous treatments on days 1, 5, 9, and 13 (indicated by arrows). Mice were observed and weighed daily; tumors were measured 2 to 3 times per week. On day 16, T/C values equaled 11%, 26%, and 28% for C1, gemcitabine, and cisplatin, respectively. Antitumor activities were recorded for C1 (T–C = 9 days; 1.9 gross $\log_{10}$ kill), gemcitabine (T–C = 7 days; 1.5 gross $\log_{10}$ kill), and cisplatin (T–C = 8 days, 1.7 gross $\log_{10}$ kill). Data are shown for the median tumor burdens of each treatment group.

are significantly expressed in NS-NSCLC, along with RFC and FRα. PCFT protein levels were increased in primary NS-NSCLC over normal lung specimens, although there was no association of PCFT levels with tumor stage. In our analysis, FRα transcripts were variably expressed in primary NS-NSCLC, and FRα was detected in only one of the NS-NSCLC cell lines (H1437). A wide range of FRα expression in NSCLC has been previously reported (Nunez et al., 2012; O'Shannessy et al., 2012; Christoph et al., 2013), suggesting that a subset of these patients might be amenable to FR-targeted therapies (Assaraf et al., 2014; Vergote and Leamon, 2015), whereas patients with lower FRα levels might be better treated with other therapies.

We demonstrated high levels of PCFT transport in five out of six NS-NSCLC cell lines, using radiolabeled PMX and C2 as surrogate substrates, accompanying detection of PCFT transcripts and proteins. Correlations between levels of PCFT transcripts and proteins, or between PCFT proteins and transport activity, were inconsistent for the NS-NSCLC cell lines, suggesting involvement of post-transcriptional and post-translational regulatory mechanisms. Similar results were previously reported for PCFT (Kugel Desmoulin et al., 2011) in a disparate panel of human tumor cell lines, implying a post-translational regulation of PCFT. For H1299 NS-NSCLC cells, a lack of detectable PCFT protein was accompanied by very low levels of transport activity. PCFT transport of PMX and C2 in H460 cells was further confirmed by PCFT knockdowns. Although in vitro C1 and C2 antitumor efficacies were significantly decreased in the PCFT KD cells, this effect was reduced for PMX, likely reflecting transport promiscuity for PMX with both PCFT and RFC.

PCFT transport of C1 and C2 into H460 cells was accompanied by inhibition of cellular GARFTase in de novo purine nucleotide biosynthesis, and resulted in inhibition of cell proliferation, even at comparatively neutral pH levels. Growth inhibition, as reflected in IC_{50} values, was generally on par with that for PMX, although increased sensitivity was measured for C1 toward A549, H460, and H2030 NS-NSCLC cells. The basis for this is unclear. In vivo C1 efficacy against an H460 tumor xenograft was also demonstrated, with T/C, T–C, and $\log_{10}$ cell kill values modestly superior to those for cisplatin and gemcitabine. These results provide proof-of-principle validation of our in vitro findings that antitumor effects of targeted C1 may be equally potent, if not more potent, than standard chemotherapies used to treat NS-NSCLC. Unfortunately, direct in vivo comparisons of C1 efficacy with PMX were not possible due to elevated serum thymidine in mice, which circumvents antitumor efficacy of TS inhibitors in the presence of thymidine kinase (van der Wilt et al., 2001).

The results of colony-forming assays with H460 cells treated with C1 and C2 at pH 6.8, conditions that approximate the pH of the tumor microenvironment (Gillies et al., 2002; Gallagher et al., 2008; Webb et al., 2011) and favor PCFT over RFC transport, were of particular interest. At pH 6.8, cytotoxicity for the 6-pyrrolo[2,3-*d*]pyrimidines C1 and C2 was clearly evident, whereas for PMX cytotoxicity was modest and incomplete up to 10 μM drug. Conversely, PMX treatment at pH 7.2 potently inhibited clonogenicity, with progressively reduced effects for C1, followed by C2. Thus, our results document selective antitumor efficacies of the novel 6-substituted pyrrolo [2,3-*d*]pyrimidine antifolates C1 and C2 compared with PMX at a pH characterizing the tumor microenvironment versus a neutral pH characteristic of most normal tissues. Accordingly, transport specificities of C1 and C2 for PCFT over RFC should confer selectivity for tumors including NS-NSCLC cells that express PCFT, which would be augmented by increased transport activity in the acidic microenvironment typical of many tumors. By this reasoning, PMX might be expected to show greater cytotoxicity than C1 or C2 toward normal tissues, where RFC transport prevails over PCFT and neutral pH favors RFC transport. As previously noted, since a subset of NS-NSCLC specimens also express significant FRα (Nunez et al., 2012; O'Shannessy et al., 2012; Christoph et al., 2013), increased tumor targeting of C1 and C2 via FRα in addition to PCFT (Wang et al., 2011, 2015) may also occur. The net effect of these targeted therapies would be increased killing of tumors, while decreasing toxicity toward normal tissues.

NSCLC is a heterogeneous disease, associated with unique genetic alterations, involving EGFR, anaplastic lymphoma tyrosine kinase (ALK), KRAS, and BRAF (Dearden et al., 2013). Among genes commonly mutated in NSCLC, it was reported that patients harboring ALK mutations experienced increased survival over other patients when treated with PMX monotherapy (Park et al., 2015), whereas patients whose tumors had mutant KRAS experienced a greater progression-free survival, compared with patients with wild-type KRAS or mutant EGFR (Sun et al., 2013). KRAS mutant sensitivity to PMX has been suggested in vitro (Moran et al., 2014). KRAS was also reported to regulate several folate-related genes including GARFTase, TS, and RFC, and KRAS mutants appear to upregulate de novo purine nucleotide biosynthesis (Moran et al., 2014), although the relationship between KRAS and PCFT has not been studied. In our study, three of the NS-NSCLC cell lines express mutant KRAS (A549, H460, and H2030) (Phelps et al., 1996; Khan and Anderson, 2001; Park et al., 2010; Moran et al., 2014) and all were less sensitive to PMX than to C1. Clearly, further detailed studies that explore sensitivities to targeted 6-pyrrolo[2,3-*d*]pyrimidine compounds such as C1 and mutant subtypes of NS-NSCLC are warranted. This will be the subject of future reports.

Authorship Contributions

Participated in research design: Wilson, Hou, Polin, Ratnam, Gangjee, Matherly.

Conducted experiments: Wilson, Hou, Yang, Kushner, White, Huang.

Performed data analysis: Wilson, Hou, Matherly.

Wrote or contributed to the writing of the manuscript: Wilson, Hou, Polin, Ratnam, Gangjee, Matherly.

References

Alati T, Worzalla JF, Shih C, Bewley JR, Lewis S, Moran RG, and Grindey GB (1996) Augmentation of the therapeutic activity of lometrexol [(6-*R*)5,10-dideazatetrahydrofolate] by oral folic acid. *Cancer Res* **56**:2331–2335.

American Cancer Society (2016) *Cancer Facts & Figures 2016*. Atlanta: American Cancer Society.

Assaraf YG, Leamon CP, and Reddy JA (2014) The folate receptor as a rational therapeutic target for personalized cancer treatment. *Drug Resist Updat* **17**: 89–95.

Boritzki TJ, Barlett CA, Zhang C, and Howland EF (1996) AG2034: a novel inhibitor of glycinamide ribonucleotide formyltransferase. *Invest New Drugs* **14**:295–303.

Budman DR, Johnson R, Barile B, Bowsher RR, Vinciguerra V, Allen SL, Kolitz J, Ernest CS, 2nd, Kreis W, and Zervos P et al. (2001) Phase I and pharmacokinetic study of LY309887: a specific inhibitor of purine biosynthesis. *Cancer Chemother Pharmacol* **47**:525–531.

Chattopadhyay S, Moran RG, and Goldman ID (2007) Pemetrexed: biochemical and cellular pharmacology, mechanisms, and clinical applications. *Mol Cancer Ther* **6**: 404–417.

Cherian C, Kugel Desmoulin S, Wang L, Polin L, White K, Kushner J, Stout M, Hou Z, Gangjee A, and Matherly LH (2013) Therapeutic targeting malignant

mesothelioma with a novel 6-substituted pyrrolo[2,3-*D*]pyrimidine thienoyl antifolate via its selective uptake by the proton-coupled folate transporter. *Cancer Chemother Pharmacol* **71**:999–1011.
Christoph DC, Asuncion BR, Hassan B, Tran C, Maltzman JD, O'Shannessy DJ, Wynes MW, Gauler TC, Wohlschlaeger J, and Hoiczyk M et al. (2013) Significance of folate receptor alpha and thymidylate synthase protein expression in patients with non-small-cell lung cancer treated with pemetrexed. *J Thorac Oncol* **8**: 19–30.
Corbett TH, LoRusso P, Demchick L, Simpson C, Pugh S, White K, Kushner J, Polin L, Meyer J, and Czarnecki J et al. (1998) Preclinical antitumor efficacy of analogs of XK469: sodium-(2-[4-(7-chloro-2-quinoxalinyloxy)phenoxy]propionate. *Invest New Drugs* **16**:129–139.
Corbett TH, Valeriote FA, Demchik L, Lowichik N, Polin L, Panchapor C, Pugh S, White K, Kushner J, and Rake J et al. (1997) Discovery of cryptophycin-1 and BCN-183577: examples of strategies and problems in the detection of antitumor activity in mice. *Invest New Drugs* **15**:207–218.
Dearden S, Stevens J, Wu YL, and Blowers D (2013) Mutation incidence and coincidence in non small-cell lung cancer: meta-analyses by ethnicity and histology (mutMap). *Ann Oncol* **24**:2371–2376.
Desmoulin SK, Hou Z, Gangjee A, and Matherly LH (2012a) The human proton-coupled folate transporter: biology and therapeutic applications to cancer. *Cancer Biol Ther* **13**:1355–1373.
Desmoulin SK, Wang L, Polin L, White K, Kushner J, Stout M, Hou Z, Cherian C, Gangjee A, and Matherly LH (2012b) Functional loss of the reduced folate carrier enhances the antitumor activities of novel antifolates with selective uptake by the proton-coupled folate transporter. *Mol Pharmacol* **82**:591–600.
Desmoulin SK, Wang Y, Wu J, Stout M, Hou Z, Fulterer A, Chang MH, Romero MF, Cherian C, and Gangjee A et al. (2010) Targeting the proton-coupled folate transporter for selective delivery of 6-substituted pyrrolo[2,3-*d*]pyrimidine antifolate inhibitors of de novo purine biosynthesis in the chemotherapy of solid tumors. *Mol Pharmacol* **78**:577–587.
Esteban E, Casillas M, and Cassinello A (2009) Pemetrexed in first-line treatment of non-small cell lung cancer. *Cancer Treat Rev* **35**:364–373.
Gallagher FA, Kettunen MI, Day SE, Hu DE, Ardenkjaer-Larsen JH, in't Zandt R, Jensen PR, Karlsson M, Golman K, and Lerche MH et al. (2008) Magnetic resonance imaging of pH in vivo using hyperpolarized 13C-labelled bicarbonate. *Nature* **453**:940–943.
Genova C, Rijavec E, Truini A, Coco S, Sini C, Barletta G, Dal Bello MG, Alama A, Savarino G, and Pronzato P et al. (2013) Pemetrexed for the treatment of non-small cell lung cancer. *Expert Opin Pharmacother* **14**:1545–1558.
Gerber DE and Schiller JH (2013) Maintenance chemotherapy for advanced non-small-cell lung cancer: new life for an old idea. *J Clin Oncol* **31**:1009–1020.
Gibbs DD, Theti DS, Wood N, Green M, Raynaud F, Valenti M, Forster MD, Mitchell F, Bavetsias V, and Henderson E et al. (2005) BGC 945, a novel tumor-selective thymidylate synthase inhibitor targeted to alpha-folate receptor-overexpressing tumors. *Cancer Res* **65**:11721–11728.
Gillies RJ, Raghunand N, Karczmar GS, and Bhujwalla ZM (2002) MRI of the tumor microenvironment. *J Magn Reson Imaging* **16**:430–450.
Hou Z, Kugel Desmoulin S, Etnyre E, Olive M, Hsiung B, Cherian C, Wloszczynski PA, Moin K, and Matherly LH (2012) Identification and functional impact of homo-oligomers of the human proton-coupled folate transporter. *J Biol Chem* **287**: 4982–4995.
Khan QA and Anderson LM (2001) Hydrocarbon carcinogens evade cellular defense mechanism of G1 arrest in nontransformed and malignant lung cell lines. *Toxicol Appl Pharmacol* **173**:105–113.
Kugel Desmoulin S, Wang L, Hales E, Polin L, White K, Kushner J, Stout M, Hou Z, Cherian C, and Gangjee A et al. (2011) Therapeutic targeting of a novel 6-substituted pyrrolo [2,3-*d*]pyrimidine thienoyl antifolate to human solid tumors based on selective uptake by the proton-coupled folate transporter. *Mol Pharmacol* **80**:1096–1107.
Laemmli UK (1970) Cleavage of structural proteins during the assembly of the head of bacteriophage T4. *Nature* **227**:680–685.
Liu Y, Yin TJ, Zhou R, Zhou S, Fan L, and Zhang RG (2013) Expression of thymidylate synthase predicts clinical outcomes of pemetrexed-containing chemotherapy for non-small-cell lung cancer: a systemic review and meta-analysis. *Cancer Chemother Pharmacol* **72**:1125–1132.
Matherly LH, Hou Z, and Deng Y (2007) Human reduced folate carrier: translation of basic biology to cancer etiology and therapy. *Cancer Metastasis Rev* **26**:111–128.
Matherly LH, Wilson MR, and Hou Z (2014) The major facilitative folate transporters solute carrier 19A1 and solute carrier 46A1: biology and role in antifolate chemotherapy of cancer. *Drug Metab Dispos* **42**:632–649.
Matsudaira P (1987) Sequence from picomole quantities of proteins electroblotted onto polyvinylidene difluoride membranes. *J Biol Chem* **262**:10035–10038.
Mendelsohn LG, Worzalla JF, and Walling JM (1999) Preclinical and clinical evaluation of the glycinamide ribonucleotide formyltransferase inhibitors lometrexol and LY309887, in *Anticancer Drug Development Guide: Antifolate Drugs in Cancer Therapy* (Jackman AL ed) pp 261–280, Humana Press, Inc., Totowa, NJ.
Moran DM, Trusk PB, Pry K, Paz K, Sidransky D, and Bacus SS (2014) KRAS mutation status is associated with enhanced dependency on folate metabolism pathways in non-small cell lung cancer cells. *Mol Cancer Ther* **13**: 1611–1624.
Nunez MI, Behrens C, Woods DM, Lin H, Suraokar M, Kadara H, Hofstetter W, Kalhor N, Lee JJ, and Franklin W et al. (2012) High expression of folate receptor alpha in lung cancer correlates with adenocarcinoma histology and *EGFR* mutation. *J Thorac Oncol* **7**:833–840.
O'Shannessy DJ, Yu G, Smale R, Fu YS, Singhal S, Thiel RP, Somers EB, and Vachani A (2012) Folate receptor alpha expression in lung cancer: diagnostic and prognostic significance. *Oncotarget* **3**:414–425.
Park IH, Kim JY, Jung JI, and Han JY (2010) Lovastatin overcomes gefitinib resistance in human non-small cell lung cancer cells with *K-Ras* mutations. *Invest New Drugs* **28**:791–799.
Park S, Park TS, Choi CM, Lee DH, Kim SW, Lee JS, Kim WS, Song JS, and Lee JC (2015) Survival benefit of pemetrexed in lung adenocarcinoma patients with anaplastic lymphoma kinase gene rearrangements. *Clin Lung Cancer* **16**: e83–e89.
Patki M, Gadgeel S, Huang Y, McFall T, Shields AF, Matherly LH, Bepler G, and Ratnam M (2014) Glucocorticoid receptor status is a principal determinant of variability in the sensitivity of non-small-cell lung cancer cells to pemetrexed. *J Thorac Oncol* **9**:519–526.
Phelps RM, Johnson BE, Ihde DC, Gazdar AF, Carbone DP, McClintock PR, Linnoila RI, Matthews MJ, Bunn PA, Jr, and Carney D et al. (1996) NCI-Navy Medical Oncology Branch cell line data base. *J Cell Biochem Suppl* **24**:32–91.
Polin L, Corbett TH, Roberts BJ, Lawson AJ, Leopold WR, White K, Kushner J, Hazeldine S, Moore R, and Rake J et al. (2011) Transplantable syngeneic rodent tumors: solid tumors, in *Mice Tumor Models in Cancer Research* (Teicher BA ed) pp 43–78, Humana Press, Totowa, NJ.
Polin L, Valeriote F, White K, Panchapor C, Pugh S, Knight J, LoRusso P, Hussain M, Liversidge E, and Peltier N et al. (1997) Treatment of human prostate tumors PC-3 and TSU-PR1 with standard and investigational agents in SCID mice. *Invest New Drugs* **15**:99–108.
Qiu A, Jansen M, Sakaris A, Min SH, Chattopadhyay S, Tsai E, Sandoval C, Zhao R, Akabas MH, and Goldman ID (2006) Identification of an intestinal folate transporter and the molecular basis for hereditary folate malabsorption. *Cell* **127**: 917–928.
Racanelli AC, Rothbart SB, Heyer CL, and Moran RG (2009) Therapeutics by cytotoxic metabolite accumulation: pemetrexed causes ZMP accumulation, AMPK activation, and mammalian target of rapamycin inhibition. *Cancer Res* **69**: 5467–5474.
Ray MS, Muggia FM, Leichman CG, Grunberg SM, Nelson RL, Dyke RW, and Moran RG (1993) Phase I study of (6*R*)-5,10-dideazatetrahydrofolate: a folate antimetabolite inhibitory to de novo purine synthesis. *J Natl Cancer Inst* **85**:1154–1159.
Rosowsky A, Bader H, Wright JE, Keyomarsi K, and Matherly LH (1994) Synthesis and biological activity of N^{ω}-hemiphthaloyl-α,ω-diaminoalkanoic acid analogues of aminopterin and 3′,5-dichloroaminopterin. *J Med Chem* **37**:2167–2174.
Shih C and Thornton DE (1999) Preclinical pharmacology studies and the clinical development of a novel multitargeted antifolate, MTA (LY231514), in *Anticancer Drug Development Guide: Antifolate Drugs in Cancer Therapy* (Jackman AL ed) pp 183–201, Humana Press, Inc., Totowa, NJ.
Sun JM, Hwang DW, Ahn JS, Ahn MJ, and Park K (2013) Prognostic and predictive value of KRAS mutations in advanced non-small cell lung cancer. *PLoS One* **8**: e64816.
Tomasini P, Greillier L, Khobta N, and Barlesi F (2013) The place of pemetrexed in the management of non-small-cell lung cancer patients. *Expert Rev Anticancer Ther* **13**:257–266.
Varela-Moreiras G and Selhub J (1992) Long-term folate deficiency alters folate content and distribution differentially in rat tissues. *J Nutr* **122**:986–991.
Vergote I and Leamon CP (2015) Vintafolide: a novel targeted therapy for the treatment of folate receptor expressing tumors. *Ther Adv Med Oncol* **7**:206–218.
Wang L, Cherian C, Desmoulin SK, Polin L, Deng Y, Wu J, Hou Z, White K, Kushner J, and Matherly LH et al. (2010) Synthesis and antitumor activity of a novel series of 6-substituted pyrrolo[2,3-*d*]pyrimidine thienoyl antifolate inhibitors of purine biosynthesis with selectivity for high affinity folate receptors and the proton-coupled folate transporter over the reduced folate carrier for cellular entry. *J Med Chem* **53**:1306–1318.
Wang L, Desmoulin SK, Cherian C, Polin L, White K, Kushner J, Fulterer A, Chang MH, Mitchell-Ryan S, and Stout M et al. (2011) Synthesis, biological, and antitumor activity of a highly potent 6-substituted pyrrolo[2,3-*d*]pyrimidine thienoyl antifolate inhibitor with proton-coupled folate transporter and folate receptor selectivity over the reduced folate carrier that inhibits β-glycinamide ribonucleotide formyltransferase. *J Med Chem* **54**:7150–7164.
Wang L, Wallace A, Raghavan S, Deis SM, Wilson MR, Yang S, Polin L, White K, Kushner J, and Orr S et al. (2015) 6-Substituted pyrrolo[2,3-*d*]pyrimidine thienoyl regioisomers as targeted antifolates for folate receptor α and the proton-coupled folate transporter in human tumors. *J Med Chem* **58**:6938–6959.
Webb BA, Chimenti M, Jacobson MP, and Barber DL (2011) Dysregulated pH: a perfect storm for cancer progression. *Nat Rev Cancer* **11**:671–677.
van der Wilt CL, Backus HH, Smid K, Comijn L, Veerman G, Wouters D, Voorn DA, Priest DG, Bunni MA, and Mitchell F et al. (2001) Modulation of both endogenous folates and thymidine enhance the therapeutic efficacy of thymidylate synthase inhibitors. *Cancer Res* **61**:3675–3681.
Xia W and Low PS (2010) Folate-targeted therapies for cancer. *J Med Chem* **53**: 6811–6824.
Zhao R and Goldman ID (2007) The molecular identity and characterization of a proton-coupled folate transporter—PCFT; biological ramifications and impact on the activity of pemetrexed. *Cancer Metastasis Rev* **26**:129–139.
Zhao R, Matherly LH, and Goldman ID (2009) Membrane transporters and folate homeostasis: intestinal absorption and transport into systemic compartments and tissues. *Expert Rev Mol* ***Med*** **11**:e4.

Address correspondence to: Dr. Larry H. Matherly, Molecular Therapeutics Program, Barbara Ann Karmanos Cancer Institute, 110 E. Warren Avenue, Detroit, MI 48201. E-mail: matherly@karmanos.org or Aleem Gangjee, Division of Medicinal Chemistry, Graduate School of Pharmaceutical Sciences, Duquesne University, 600 Forbes Avenue, Pittsburgh, PA 15282. E-mail: gangjee@duq.edu